

Wave–Packet Scattering off the Kink–Solution

A. M. H. H. Abdelhady and H. Weigel

Physics Department, Stellenbosch University, Matieland 7602, South Africa

We investigate the propagation of a wave–packet in the ϕ^4 model. We solve the time–dependent equation of motion for two distinct initial conditions: The wave–packet in a trivial vacuum background and in the background of the kink soliton solution. We extract the scattering matrix from the wave–packet in the kink background at very late times and compare it with the result from static potential scattering in the small amplitude approximation. We vary the size of the initial wave–packet to identify non–linear effects as, for example, the replacement of the center of the kink.

PACS numbers: 03.50.-z,03.50.Kk,03.65.Nm,03.65.nk

I. INTRODUCTION

Non–linear models with soliton solutions [1] possess a wide range of applications in physics. To present an incomplete list, this range covers cosmology [2, 3], particle and nuclear physics [4, 5], as well as condensed matter physics [6]. The kink–model in one time and one space dimension for the real scalar field ϕ

$$\mathcal{L} = \frac{1}{2} \partial_\mu \phi \partial^\mu \phi - \frac{\lambda}{4} \left(\phi^2 - \frac{M^2}{2\lambda} \right)^2 \quad (1)$$

is a prototype model with a topological soliton solution based on spontaneous symmetry breaking. Any feature observed in this model is likely to be relevant for the above mentioned applications.

In the Lagrangian, eq. (1) M is the mass parameter and λ is the coupling constant. The soliton solution is the so–called *kink*

$$\phi_K(x) = \frac{M}{\sqrt{2\lambda}} \tanh \left(\frac{M}{2} x \right). \quad (2)$$

It depends on the spatial coordinate but is time–independent and interpolates between the degenerate vacuum configurations $\phi_0 \equiv \pm \frac{M}{\sqrt{2\lambda}}$, that arise from spontaneous symmetry breaking. Any deviation from either of these two values at spatial infinity causes the total energy

$$E = \int_{-\infty}^{\infty} dx \epsilon(x, t) \quad \text{with} \quad \epsilon(x, t) = \frac{1}{2} \left(\dot{\phi}^2(x, t) + \phi'^2(x, t) \right) + \frac{\lambda}{4} \left(\phi^2(x, t) - \frac{M^2}{2\lambda} \right)^2, \quad (3)$$

to diverge. Here we have introduced the partial derivatives as $\dot{\phi} = \partial\phi/\partial t$ and $\phi' = \partial\phi/\partial x$. For later use, we have made the time dependent energy density, $\epsilon(x, t)$ explicit. Since such divergences may not occur when continuously converting one configuration into another, any smooth deformation cannot alter the field configuration at spatial infinity. In particular it conserves the difference $\phi(-\infty, t) - \phi(\infty, t)$. This difference may thus be viewed as a

topological charge. With proper normalization, the kink carries topological charge one, while the vacuum configuration $\phi(x, t) \equiv \phi_0$ has charge zero.

Commonly small amplitude fluctuations about the kink, $\phi(x, t) = \phi_K(x) + \eta(x, t)$ are introduced to determine scattering data. The small amplitude wave-function $\eta(x, t)$ obeys a Schrödinger type equation with a space-dependent potential induced by the kink. In this small amplitude approximation quadratic and higher orders in $\eta(x, t)$ are omitted when substituted into \mathcal{L} . At spatial infinity, *i.e.* far away from the kink, this Schrödinger equation is a Klein–Gordon equation with mass M . Application of standard methods [1] to this Schrödinger problem yield the phase shift¹

$$\delta(k) = 2\arctan\left(\frac{3Mk}{2k^2 - M^2}\right). \quad (4)$$

The generalization to three spatial dimensions is that of meson–baryon scattering [7]. The kink ϕ_K represents the baryon and the fluctuations η are mesons [8].

In this paper we show how the same result for the phase shift can be obtained from the physically motivated set-up of a wave-packet interacting with the kink. This exactly matches the scenario that a meson scatters off a baryon. In particular, we construct the wave-packet such that at spatial infinity the field equals either of the possible vacuum configurations for any finite time t . In this set-up we will numerically solve the time dependent equation of motion

$$\ddot{\phi}(x, t) = \phi''(x, t) - \lambda \left(\phi^2(x, t) - \frac{M^2}{2\lambda} \right) \phi(x, t) \quad (5)$$

with appropriate initial and boundary conditions for $\phi(x, t)$. The total energy, eq. (3) of configurations that obey this equation of motion stays constant in time.

Numerical simulations of the time-dependent solutions in the kink model have been around since quite a while. For example, the transition time of a wave-packet through the kink was estimated in ref. [9]. This occurred in the greater context of modeling phase transitions. The resonance structure of the kink–antikink interaction was numerically studied in ref. [10]. Lattice studies of the kink model were reported in ref. [11, 12] as a simulation of molecular dynamics. These numerical studies focus on kink–antikink configurations which belong to the topological trivial sector. More recently this sector has undergone numerical investigation in the context of pair-creation [13], electro-weak oscillons [14, 15] and bounces [16, 17]. Numerical simulations within the 2 + 1 dimensional generalization at non-zero temperature allowed to study the effect of fast quenches to model resonant nucleation [18]. This scenario may have applications in condensed matter and cosmology [19]. Within super-symmetric extensions of the kink model, numerical simulations have even been used to study brane world collisions [20–22]. In the unit topological charge sector numerical simulations have been employed to investigate the effect of impurities in the kink [23]. However, no study in the sector of unit topological charge is known to us that attempts to extract the scattering phase shift from the time-dependent differential equation or to identify non-linear effects in this sector by going beyond the small amplitude approximation for the scattering process.

¹ Since the induced potential is reflectionless, the two eigenphase shifts are identical.

This short paper is organized as follows. In the next section we describe the set-up for the wave-packet, *i.e.* we specify the initial and boundary conditions to solve the time dependent equation of motion (5). In principle, a single integration of this equation can, after Fourier transformation, provide information on scattering data for all momenta. In section III we will discuss the numerical simulation of the time-dependent configuration and describe how the scattering phase shift can be extracted. We will observe structural changes of the interaction pattern as the amplitude of the initial wave-packet increases. We conclude in section IV.

II. WAVE-PACKET

We will consider wave-packets in the two sectors of vanishing and of unit topological charges. Their structures are generic and we merely have to specify the background fields for either of the two cases.

As initial condition for the wave-packet we consider a linear combination of plane waves that satisfy the Klein-Gordon dispersion relation, $\omega_k = \sqrt{k^2 + M^2}$. Hence at $t = 0$ we parameterize

$$\eta_{\text{wp}}(x) = \int_{-\infty}^{\infty} dk A(k) e^{ikx}. \quad (6)$$

At $t = 0$ the dispersion relation enters only via the velocity of the initial wave-packet

$$\dot{\eta}_{\text{wp}}(x) = -i \int_{-\infty}^{\infty} dk \omega_k A(k) e^{ikx}. \quad (7)$$

In the context of our numerical simulations we assume the spectral function in momentum space to be of Gaussian shape

$$A(k) = a_0 e^{-\frac{(k-k_0)^2}{\sigma_k^2}}, \quad (8)$$

where a_0 is the amplitude, k_0 is the average momentum, and σ_k is the width of the distribution. Though the momentum integral in eq. (6) can be straightforwardly computed, we refrain from displaying it here because its analog in eq. (7) has no closed representation. We compute either of the integrals numerically. We remark that $\eta_{\text{wp}}(x)$ may exhibit oscillations since it is a complex Gaussian distribution. This is especially the case when σ_k is not particularly large. The distribution is centered around $x = 0$ and $\dot{\eta}_{\text{wp}}(x)$ increases with k_0 , which measures the average velocity with which the wave-packet propagates.

As the equation of motion is second order in time, we have completely determined the initial conditions for the wave-packet in eqs. (6) and (7). We next super-impose it with various background configurations that solve the static equation of motion. Such combinations serve as initial configurations to integrate the equation of motion (5). By construction, the initial wave-packet is localized and since the total energy is conserved, the topological charge of this super-imposed configuration will be that of the background.

A. Pure wave–packet

For the pure wave–packet we merely consider the above defined distribution around the trivial vacuum at early times

$$\phi(x, 0) = \frac{M}{\sqrt{2\lambda}} + \eta_{\text{wp}}(x) \quad \text{and} \quad \left. \frac{\partial \phi(x, t)}{\partial t} \right|_{t=0} = \dot{\eta}_{\text{wp}}(x) \quad (9)$$

and feed it into the equation of motion (5). Since the velocity $\dot{\eta}_{\text{wp}}(x)$ is characterized by the dispersion relation extracted from eq. (5), the superposition

$$\phi(x, t) = \frac{M}{\sqrt{2\lambda}} + \int_{-\infty}^{\infty} dk A(k) e^{i(kx - \omega_k t)} \quad (10)$$

is an approximate solution as long as a_0 is small enough to neglect $\mathcal{O}(\eta_{\text{wp}}^2)$ terms in the equation of motion. This omission defines the small amplitude approximation. As we increase a_0 non–linear effects emerge and the solution to the differential equation will no longer be a superposition of plane waves.

We may converse this line of argument to study non–linear effects. Assume $\phi(x, t)$ to be the (numerical) solution to the equation of motion that emerges from the above defined initial condition. Then the deviation of the Fourier transform

$$\tilde{\phi}_{t_f}(k) = \frac{e^{i\omega_k t_f}}{A(k)} \int_{-\infty}^{\infty} \frac{dx}{2\pi} e^{-ikx} \left[\phi(x, t_f) - \frac{M}{\sqrt{2\lambda}} \right] \quad (11)$$

from unity measures non–linear effects for times $t_f \gg 0$. Obviously, a single integration of the equation of motion in coordinate space provides information about the full momentum space.

B. Wave–packet in kink background

For the wave–packet with unit topological charge in the kink background we consider the initial configuration

$$\phi(x, 0) = \phi_{\text{K}}(x - x_0) + \eta_{\text{wp}}(x) \quad (12)$$

where x_0 is the position of the center of the kink soliton solution. It must be taken large enough to avoid any overlap between the kink and the wave–packet at $t = 0$ if we want to discuss the scattering problem. In order for scattering to occur, the signs of x_0 and k_0 must coincide. Otherwise the wave–packet will propagate away from the kink². Since the kink is static, the initial velocity is as in eq. (7). Any non–zero velocity of the kink can eventually be compensated by an appropriate Lorentz transformation [1], that modifies the details but not the structure of the wave–packet.

Again, we can give an analytical expression for the solution to this initial condition, provided we may omit $\mathcal{O}(\eta_{\text{wp}}^2)$ terms according to the small amplitude approximation

$$\phi(x, t) = \phi_{\text{K}}(x - x_0) + \eta_{\text{wp}}^{(S)}(x, t), \quad (13)$$

² The wave–packet contains components with negative momenta. They do not participate in scattering for our choice $x_0 > 0$.

where

$$\eta_{\text{wp}}^{(S)}(x, t) = \int_{-\infty}^{\infty} dk A(k) \exp [i (kx - \omega_k t + \delta(k))] . \quad (14)$$

As for the pure wave-packet, our analysis will be converse. We prescribe the spectral function $A(k)$ as in eq. (8) together with the dispersion relation associated with the Klein-Gordon equation. This enters the initial configurations $\phi(x, 0)$ and $\dot{\phi}(x, 0)$ and we utilize the equation of motion, eq. (5) to find the time-dependent configuration, $\phi(x, t)$. We then consider very late times $t_f \gg 0$ at which the wave-packet has completely penetrated the kink and the two structures are again well separated and can be individually identified. This defines the late-time wave-packet type solution

$$\eta_{\text{wp}}^{(S)}(x, t_f) = \phi(x, t_f) - \phi_{\text{K}}(x - x_0) . \quad (15)$$

Its (inverse) Fourier transform should be compared with the small-amplitude solution, eq. (14)

$$\int_{-\infty}^{\infty} \frac{dx}{2\pi} e^{-ikx} \eta_{\text{wp}}^{(S)}(x, t_f) = A(k) \exp [i (\delta(k) - \omega_k t_f)] + \mathcal{O}(a_0^2) . \quad (16)$$

That is, from the numerical solution to the equation of motion we should be able to extract the phase shift

$$e^{i\delta(k)} = \frac{e^{i\omega_k t_f}}{A(k)} \int_{-\infty}^{\infty} \frac{dx}{2\pi} e^{-ikx} \eta_{\text{wp}}^{(S)}(x, t_f) . \quad (17)$$

As long as $\eta(x, t)$ satisfies the criteria for a small amplitude fluctuation, the dependence on t_f cancels on the right hand side. A main purpose of the present investigation is to compare the numerical result, eq. (17), for the components that participate in scattering, with the result from small amplitude approximation in eq. (4).

III. NUMERICAL RESULTS

Appropriate scaling of the coordinates and the field

$$(x, t) \longrightarrow \frac{(x, t)}{\sqrt{2} M} \quad \text{and} \quad \phi \longrightarrow \frac{M}{\sqrt{2} \lambda} \phi \quad (18)$$

allows us to completely absorb the model parameters. Hence their actual values are of minor relevance and all results are genuine. In this section we will quote all numerical results in terms of the dimensionless quantities on the right hand side of eq. (18). In these units the vacuum solutions are at $\phi_0 = \pm 1$ and the small amplitude fluctuations have mass $\sqrt{2}$.

The numerical treatment starts by defining an equi-distant grid with spacing h in coordinate space. This establishes an interval on the x -axis that we take to be finite but much larger than the extension of the wave-packet and the kink. Then we employ a fourth order Runge-Kutta algorithm together with an adaptive step size control to solve the equation of motion (5). The latter considerably slows down the numerical computation as the amplitude a_0 is increased. Earlier attempts using a simple Euler algorithm failed to produce acceptable accuracy. The equation of motion propagates the configuration in time. At each time step (as well as at the auxiliary intermediate steps required by the Runge-Kutta algorithm) we compute the (second) spatial derivative of the configuration that occurs on the

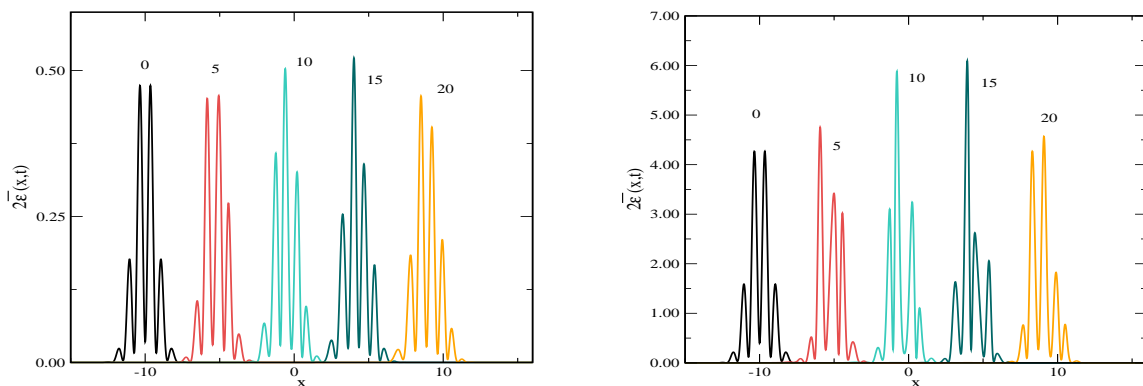


FIG. 1: (Color online) Time snapshots of the energy density $\bar{\epsilon}(x, t)$ (in $M^4/8\lambda^2$) of the wave-packet for real initial conditions. We have used $k_0 = 4$ and $\sigma_k = 2$. Left panel: $a = 0.05$, right panel: $a = 0.15$. The numbers next to the lines refer to the time variable. Note the different scales on the ordinate.

right-hand-side of the equation of motion with an $\mathcal{O}(h^4)$ accuracy. To this end, the configuration is assumed to vanish at points outside the considered interval in coordinate space. This corresponds to the boundary condition that no flux penetrates outside this interval. As a consequence thereof, the wave-packet bounces at the spatial boundaries after very long times. This is, of course, not physical but merely a finite size effect and we have to terminate the simulation at late times when this phenomena becomes visible.

A major criterion to accept the numerical solution is that the total energy, eq. (3) stays constant in time (at the order of the desired numerical accuracy). The complex wave-packet initial condition implies the total energy and the energy density to be complex as well. The investigation of the physical energy density, $\epsilon(x, t)$ in eq. (3) hence requires to also solve the equation of motion with the real initial condition

$$\eta_R(x) = \int_{-\infty}^{\infty} dk A(k) \cos(kx) \quad \text{and} \quad \dot{\eta}_R(x) = \int_{-\infty}^{\infty} dk \omega_k A(k) \sin(kx) \quad (19)$$

for the wave-packet. In figures (1) and (2) we display the time evolution of the subtracted energy density

$$\bar{\epsilon}(x, t) = \epsilon(x, t) - \epsilon_{\text{bg}}(x) \quad (20)$$

for this initial condition. To single out the wave-packet contribution, we have subtracted the energy density associated with the static background. For the pure wave-packet this is zero but with the kink background we have $\epsilon_{\text{bg}}(x) = \frac{1}{2} \left[1 - \tanh^2 \left(\frac{x-x_0}{\sqrt{2}} \right) \right]^2$ in the dimensionless units of eq. (18). In the context of the small amplitude approximation the kink is assumed to be infinitely massive and thus does not change its location during the interaction³. We observe an interesting effect at the center of the kink. Once the wave-packet has passed by, a residual deformation of the energy density remains. This effect persists even for very long

³ In the three dimensional scenario of meson baryon scattering this resembles the large N_C picture in which the baryon is $\mathcal{O}(N_C)$ heavier than the meson.

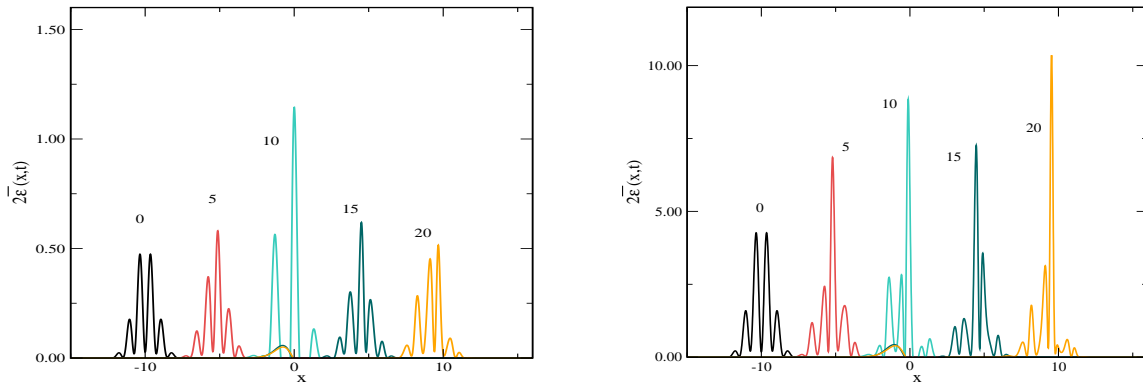


FIG. 2: (Color online) Same as figure 1 with the kink background.

times and becomes stable. Also, it is the more pronounced the larger the amplitude of the wave–packet is. We will discuss a potential explanation for this effect in subsection B.

The energy density associated with the wave–packet in particular suggests to discuss its spread by first defining the normalized expectation values

$$\langle x^n \rangle = \frac{\int dx x^n \bar{\epsilon}(x, t)}{\int dx \bar{\epsilon}(x, t)}. \quad (21)$$

This enables the computation of the (squared) standard deviation

$$\sigma^2 = \langle x^2 \rangle - \langle x \rangle^2 \quad (22)$$

as a direct measure for the width of the wave–packet. The time–dependence of the position of the center $\langle x \rangle$ is essentially unaffected by the kink as the data in table I show. Furthermore its velocity agrees with what is expected for the wave–packet as $\frac{k_0}{\sqrt{k_0^2+2}} \approx 0.94$ for $k_0 = 4$.

We find the total energy stored in the wave–packet to be 0.52 and 4.65 for $a_0 = 0.05$ and $a_0 = 0.15$, respectively. The latter corresponds to more than three times the mass of a Klein–Gordon particle. Non–linear effects for $\langle x \rangle$, *i.e.* its dependence on a_0 , are only marginal. We compare the results for σ from different values of the amplitude a_0 in both cases, with and without the kink background, in table II. Obviously the kink background causes a significant increase of the spread of the wave–packet. Closer inspection shows that this manifests itself mainly after the interaction between the wave–packet and the kink, that is for $t > 10$ while even up to the time of the interaction no significant difference between the cases with and without the kink is observed. We assert the strong increase of σ after the interaction to the emergence of the above mentioned structure around $x \approx x_0$ rather than to a direct spread of the wave–packet. Indeed, the comparison between figures 1 and 2 does not indicate a severe increase of the spread.

A. Propagation of pure wave–packet

We now return to the complex valued initial wave–packet. We first consider the pure wave–packet, eq. (9). The simulation of eq. (11) will provide information about the numerical accuracy that we can expect when attempting to extract the phase shift at a later stage.

		w/o kink		w/ kink	
$t \backslash a_0$		0.05	0.15	0.05	0.15
0		-10.00	-10.00	-10.00	-10.00
5		-5.28	-5.29	-5.28	-5.27
10		-0.56	-0.58	-0.55	-0.55
15		4.15	4.13	4.17	4.17
20		8.87	8.83	8.89	8.90

TABLE I: The central position $\langle x \rangle$ of the wave-packet as a function of time for $k_0 = 4$ and $\sigma_k = 2$.

		w/o kink		w/ kink	
$t \backslash a_0$		0.05	0.15	0.05	0.15
0		0.72	0.72	0.72	0.73
5		0.74	0.79	0.74	0.79
10		0.77	0.95	0.80	0.97
15		0.84	1.16	1.65	1.81
20		0.91	1.38	2.25	2.50

TABLE II: The normalized standard deviation, σ , as a function of time. Parameters are as for table I.

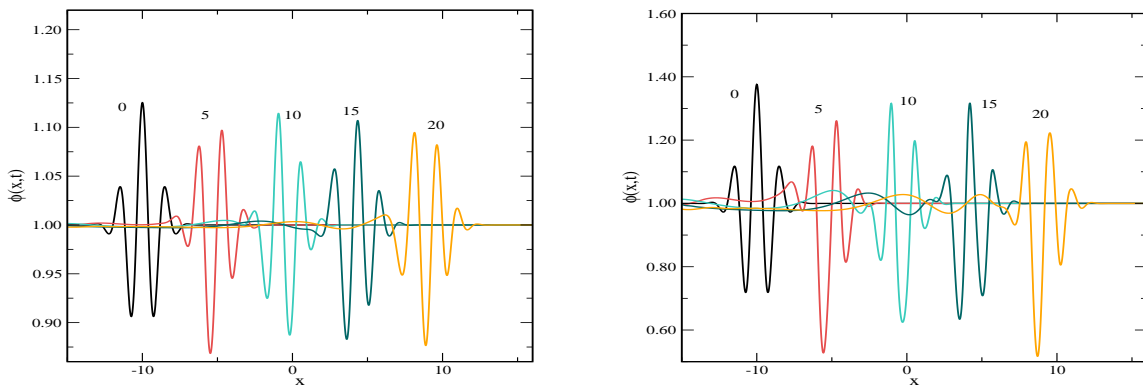


FIG. 3: (Color online) Time snapshots of the real part of the configuration $\phi(x, t) - M/\sqrt{2\lambda}$ for the initial condition, eq. (12). Furthermore we have used $k_0 = 4$ and $\sigma_k = 2$ to characterize the wave-packet. Left panel $a_0 = 0.05$, right panel $a_0 = 0.15$. Note the different scales on the ordinate.

Figure 3 shows the real parts of the numerical solution to the equation of motion for two different values of the amplitude a_0 . The imaginary part behaves similarly, just phase shifted by $\pi/2$. Note also that in addition to the expected spread, the number of (visible) oscillations contained within the wave-packet increases with time.

From the comparison of the two graphs in figure 3 no significant dependence on the initial amplitude of the form of the wave-packet can be deduced. This confirms the results for the standard deviation listed in table II. This absence of significant non-linear effects is somewhat surprising. Rather they were expected as a signal for particle production, as sufficient energy is available.

In figure 4 we show the inverse Fourier transform defined in eq. (11). As indicated above its deviation from unity provides insight in the numerical accuracy that we can achieve, at least for small a_0 . At low momenta deficiencies arise because these contributions have left the bulk of the wave-packet. Furthermore small errors at low and large momenta are amplified as $1/A(k)$ is large in these regimes. The deficiencies at small momenta are obviously independent of a_0 . This is not the case for those at large momenta, even though their structures are very similar. In this momentum regime they originate from the inverse Fourier

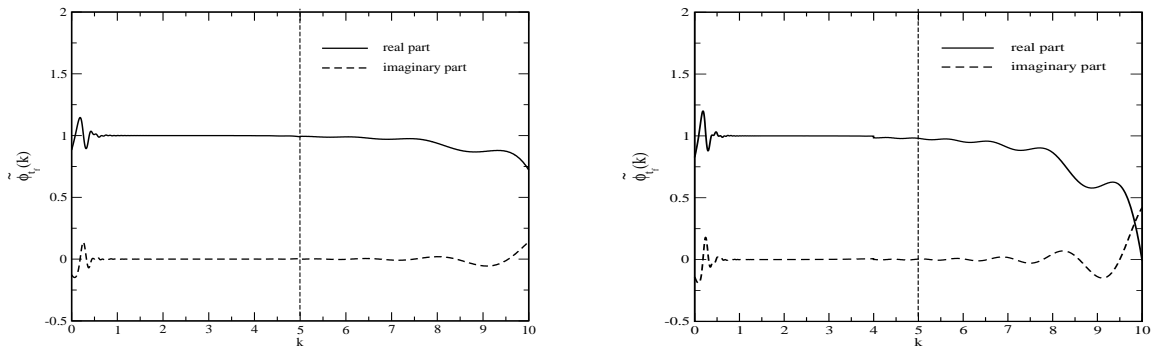


FIG. 4: The inverse Fourier transform of eq. (11) for $a_0 = 0.05$ (left) and $a_0 = 0.20$ (right). The dashed vertical lines separate regimes with different numerical parameters to improve the numerical accuracy.

transform requiring a very fine grid, *i.e.* small h , in coordinate space. Unfortunately this comes with a heavy computational cost and it occurs appropriate to divide the momentum axis into subintervals that are treated with different numerical parameters. This not only concerns the parameters for numerically solving the equation of motion (*e.g.* the step size h) but also the detailed structure of the wave-packet that we characterize by k_0 and σ_k . At the interface of these subintervals the results extracted from the different numerical treatments match. This is also indicated in figure 4. At this stage it is difficult to judge whether the deficiencies at large k are of numerical origin or signals of the non-linear dynamics.

B. Propagation in kink background

In figure 5 we present solutions to the numerical integration of the equation of motion at different times for small and moderate initial amplitudes of the wave-packet. At all times, the deviation from the kink is confined within a spatial regime. We clearly identify the interaction process when the wave-packet *climbs* up the kink. A wave-packet with a small amplitude essentially retains its shape after the interaction, the only effect being characterized by the phase shift that we will extract later. Surprisingly, even for moderate amplitudes the shape of the wave-packet does not change significantly with time.

Figure 5 has the potential to explain why the energy density $\bar{\epsilon}$ developed some structure around $x = x_0$ after the interaction with the kink: The kink acquires a displacement d . This displacement increases with the initial amplitude a_0 . We quantify this increase by identifying the point d at which $\phi(d, t) = 0$ in the vicinity of x_0 for very late times. We list d for various values of $a_0 \leq 0.2$ in table III. In agreement and support for the small amplitude approximation, the displacement vanishes with the amplitude. For moderate a_0 it saturates after a while and stays constant; at least at the order of our numerical accuracy⁴. As a_0 increases further, the displacement changes sign and slowly grows with time. This is the onset of a novel non-linear effect that we will discuss further in subsection III D. Our numerical simulations suggest that d does not depend on k_0 .

⁴ On the overall scale this displacement is an effect at the order of a fraction of a percent.

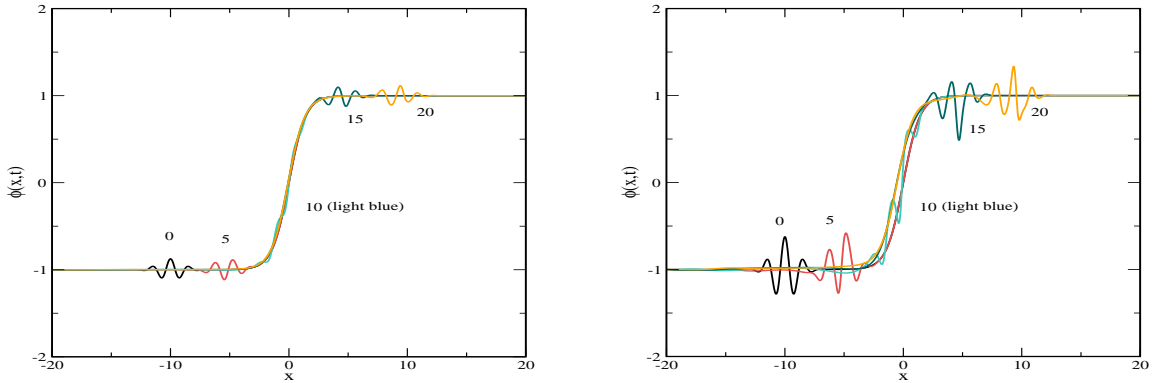


FIG. 5: (Color online) Time snapshots of the real part of the configuration $\phi(x,t)$ for the initial condition, eq. (13). Left panel $a_0 = 0.05$, right panel $a_0 = 0.15$.

	t=100				t=150				t=200			
a_0	0.05	0.10	0.15	0.20	0.05	0.10	0.15	0.20	0.05	0.10	0.15	0.20
d	-0.07	-0.40	-0.80	1.32	-0.07	-0.39	-1.13	2.80	-0.07	-0.40	-1.09	3.05

TABLE III: Displacement, d measured relative to x_0 , of the kink as a function of the initial amplitude of the wave-packet, a_0 .

For negative d the numerically observed structure (see figure 2) of $\bar{\epsilon}(x,t)$ in the vicinity of x_0 is reasonably reproduced by $\epsilon_{\text{bg}}(x-d) - \epsilon_{\text{bg}}(x)$, *i.e.* the corresponding shift of the background energy density. The larger the time interval the better is the agreement with this analytic expression. To separate the displacement effect and to focus on the time-evolution of the wave-packet we repeat the calculation of eqs. (21) and (22) with the lower boundaries of the integrals taken between the kink and wave-packet as we can separate these structures unambiguously. The results are shown in table IV. The comparison with the time-evolution of the wave-packet in the trivial background reveals that the interaction with the kink has only a minor influence on the spread of the wave-packet once the displacement of the kink is

		w/o kink				w/ kink			
		$\langle x \rangle$		σ		$\langle x \rangle$		σ	
t	a_0	0.05	0.15	0.05	0.15	0.05	0.15	0.05	0.15
50		37.2	37.1	1.54	2.92	37.5	37.2	1.40	2.28
100		84.4	84.2	2.71	5.28	84.8	85.3	1.84	4.90
150		131.5	131.3	3.89	7.61	132.1	132.8	2.22	7.93
200		178.7	178.4	5.09	9.92	179.3	180.2	4.94	11.40

TABLE IV: Center and spread of the wave-packet in the kink background for very late times. We compare the two cases with the vacuum and the kink backgrounds. In either case we have used $k_0 = 4$ and $\sigma_k = 2$ with real initial conditions.

properly accounted for. In both cases the spread increases with the amplitude of the wave-packet. This summarizes the main features of the wave-packet for small and moderate amplitudes. For $a_0 > 0.2$ we observe a different behavior that we will discuss later.

C. Extraction of phase shift

Finally we turn to a major subject of this investigation, the extraction of the phase shift from the scattering process. Comparison with the result, eq. (4), in the small amplitude approximation serves as a crucial test for the quality of the numerical solution to the time-dependent equation of motion.

Numerically solving the equation of motion (5) to determine the full momentum dependence of the phase shift faces various obstacles. First we have to incorporate the above mentioned displacement of the kink in the integral, eq. (17). This is straightforwardly accomplished by restricting the integration interval to the regime of the wave-packet. For very late times ($t_f > 100$) this regime is clearly separated from the kink. Other obstacles are more cumbersome. Wave-packet components with small momenta take a long time to finalize the interaction with the kink. Hence we need to solve the equation of motion for a large interval on the time axis. In the dimensionless units defined above we consider $t \in [0, 200]$. We also vary the upper limit to ensure stability of the results. However, components with large momenta will propagate a long distance in the same time interval. Hence we also need to consider a large interval in coordinate space. In order to reliably find the Fourier transform, eq. (16) we require a dense grid in coordinate space for large momentum components. This increases the numerical cost additionally. To keep the numerical effort within a manageable range, it is therefore appropriate to split the computation in (at least) two parts. To extract the phase shift for small momenta, we consider a large time interval but a small interval in coordinate space. This leads to unreliable results at large momenta. For that regime we consider a small time interval but a large one in coordinate space; together with a dense grid. At intermediate momenta the two procedures yield identical results. Furthermore we have the freedom to tune the parameters of the wave-packet, k_0 and σ_k to suit the considered regime in momentum space. These issues are indicated in figure 6. In that figure we have matched two numerical treatments at $k = 5$. We also display the numerical result for the imaginary part of the right hand side of eq. (16). Its deviation from unity serves as a further test on the numerical accuracy. As expected this occurs for very small and very large momenta. Otherwise the agreement with the analytical result, eq. (4) is astonishing. Certainly, further segmentation of the momentum axis and optimization in each segment will yield even better agreement. We have obtained the result displayed in figure 6 for a small amplitude ($a_0 = 0.05$) for which the small amplitude approximation is expected to be accurate. Figure 6 shows that we find identical phase shifts for different amplitudes a_0 . Though we find differences in the imaginary part of the phase shift, we believe them to be short-comings of the numerical procedure and conclude that the scattering data do not exhibit non-linear effects even at moderate amplitudes.

D. Non-linear effects in the kink background

As indicated in section II the extraction of the phase shift relies on the small-amplitude assumption. If $\mathcal{O}(\eta_{\text{wp}}^2)$ effects are not negligible we cannot expect the right-hand-side of

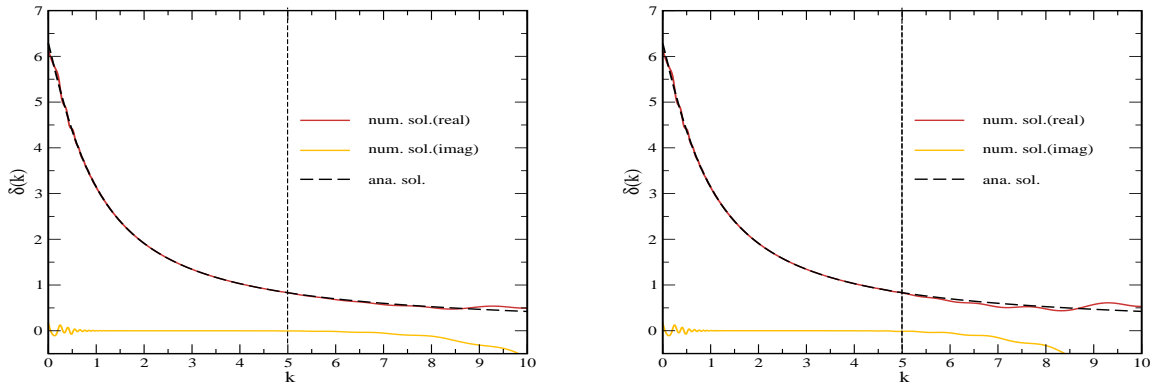


FIG. 6: (Color online) Extraction of the phase shift for various momentum regimes. Left panel: $a_0 = 0.05$, right panel: $a_0 = 0.15$. Different numerical parameters serve to improve the agreement with the analytical result in two distinct regimes. Left regime: optimized for small and moderate momenta, right regime: optimized for large momenta.

eq. (17) to have unit magnitude. Rather we expect it to be less than one, corresponding to particle production. Yet we did not observe this effect even for moderate amplitudes, since the wave-packet remains compact, *cf.* figure 5. For moderate amplitudes we have identified a small displacement of the kink as the single major effect of the non-linear dynamics. It corresponds to an attraction shortly before and a repulsion shortly after the interaction with the wave-packet.

This displacement also complicates the extraction of that part of the energy density, $\bar{\epsilon}(x)$ that is associated with the wave-packet. Once this is properly done, $\bar{\epsilon}(x)$ serves as a probability distribution of the wave-packet. The propagation of its center does not exhibit consequences of the non-linear dynamics either. This propagation is not significantly altered by the presence of the kink. However, the spread of the wave-function shows some increase with the amplitude of the wave-packet.

We show the typical behavior of the energy density, $\bar{\epsilon}(x, t)$ in figure 7 as we further increase the amplitude. Surprisingly, there is no footprint from the kink at x_0 . Instead we observe that the energy density splits into two pieces of different velocities and there is a dominant peak in $\bar{\epsilon}(x, t)$ at the back of the more quickly propagating piece. The field configuration itself reveals the answer to this peculiarity. First we observe that also the wave-packet splits in (at least) two pieces of different velocities. This is an indication for particle production. Actually we also observe such splitting for the trivial background, however, it sets in at somewhat larger amplitude⁵. More notably, the transition from one vacuum configuration ($\phi_0 = -1$) to the other ($\phi_0 = 1$), which is required to occur somewhere by conservation of the topological charge, now emerges at the back of the dominant piece of the wave-packet rather than at the position of the kink before the interaction. Obviously the dominant peak in $\bar{\epsilon}(x, t)$ results from the kink being dragged by the wave-packet. As a pronounced non-linear effect we find the transition from a stationary kink to a co-moving kink as the amplitude exceeds a certain value a_c . We extract this value from the behavior of the energy

⁵ For the vacuum background we did not observe it for $a_0 = 0.25$ but for $a_0 = 0.35$.

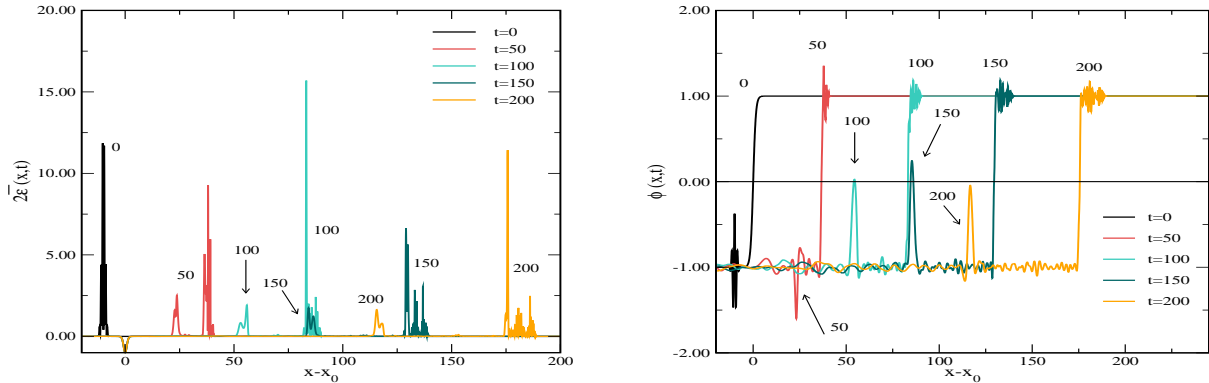


FIG. 7: (Color online) Results for real initial conditions using $a_0 = 0.25$. The numbers next to the lines refer to the time variable. Note that the second structure at $t = 150$ is partially covered by the main structure at $t = 100$. Left panel: subtracted energy density $\bar{\epsilon}(x, t)$, right panel: field configuration $\phi(x, t)$.

density. When a structure persists at a value of $d \approx x_0$ that varies only marginally in time the kink is considered to be stationary. Disappearance of this structure provides the critical value. For $k_0 = 4$ and $\sigma_k = 2$ we find $a_c = 0.201$. Obviously, it is impossible to extract scattering data from these structures. This is even more the case as parts of the initial wave-packet now trail after the kink.

IV. SUMMARY AND OUTLOOK

We have performed numerical simulations in the kink-soliton model. In particular we have set up the initial conditions to investigate the interaction of the kink with a wave-packet. Within this approach we have reconstructed the phase shift known from potential scattering in the small amplitude approximation. By choosing a significantly wide initial spectral function (in momentum space) this turned possible by a single integration of the equation of motion in coordinate space. However, numerical accuracy can be improved by optimizing both, numerical parameters and initial conditions, to a special momentum regime. This technique makes no particular reference to the background configuration and can hence be employed to other cases for which no analytic result is available. Although our technique also captures non-linear effects we did not observe them for the phase shift in the regime of small and moderate amplitude of the wave-packet. In this regime the kink does not pick up any energy from the wave-packet. However, the kink gets slightly displaced as a result of the interaction. Surprisingly, the displacement is opposite to the propagation direction of the kink. This displacement occurs as attraction before and repulsion after the interaction. Upon further increase of the amplitude the kink indeed picks up kinetic energy and gets dragged by the wave-packet. This is our main result regarding the search for effects of the non-linear dynamics. We interpret this effect as a signal for the existence of a critical strength of the amplitude beyond which the attraction between the wave-packet and the kink inescapable. Once the kink co-moves with the wave-packet, the scattering process cannot be uniquely identified nor can a phase shift be extracted. Furthermore the wave-packet splits into distinct pieces for sufficiently large amplitudes. We interpret this

splitting as particle production. It is also a consequence of the non-linear dynamics because it is equally observed without the kink background.

Eventually we want to use these numerical methods to further study the interaction of a kink-antikink system. The comparison with the above results should shed some light on whether and how crossing symmetry manifests itself in (topological) soliton models. This is a challenging problem because unlike in perturbative calculations it does not simply imply the rotation of Feynman diagrams but rather relates topologically distinct sectors that are not connected by smooth transformations. The numerical analysis will closely follow the study of refs. [13, 24]. The kink-antikink system is known to exhibit distinct features [10, 25], depending on whether or not the relative velocity exceeds the critical value $v_c = 0.2598$. Below v_c the kinetic energy is not large enough to overcome the kink-antikink attraction and a second interaction occurs. Above v_c the kinetic energy overcomes the barrier that causes the attraction. It will be interesting and challenging to establish a connection between the critical value of the amplitude (a_c) for the kink to take up kinetic energy and the above mentioned critical velocity (v_c). The existence of such a connection seems possible because both scenarios reflect a critical strength for sufficient attraction to result from the non-linear interaction within the model.

The kink induces two bound states, one with energy $\omega_1 = \sqrt{3} \frac{M}{2}$ and another (half-bound state) with energy $\omega_1 = \sqrt{2}M$ [1]. It will be interesting to see whether there are connections between these bound states and the co-moving kink. If so, this co-moving object would correspond to an excited state of the kink.

Acknowledgments

One of us (AMHHA) is supported in parts by the African Institute for Mathematical Sciences (AIMS).

-
- [1] R. Rajaraman, *Solitons and Instantons*. North Holland, Amsterdam (1982).
 - [2] A. Vilenkin and E.P.S. Shellard, *Cosmic Strings and other Topological Defects*, Cambridge University Press, Cambridge (UK), (1994).
 - [3] T. Vachaspati, *Kinks and domain walls: An introduction to classical and quantum solitons*, Cambridge University Press, Cambridge (UK), (2006).
 - [4] N. Manton and P. Sutcliffe, *Topological Solitons*, Cambridge University Press, Cambridge, (UK), (2004).
 - [5] H. Weigel, Lect. Notes Phys. **743** (2008) 1.
 - [6] A. R. Bishop and T. Schneider (Eds.), *Solitons in Condensed Matter Physics*, Springer Verlag, Berlin (1978).
 - [7] B. Schwesinger, H. Weigel, G. Holzwarth and A. Hayashi, Phys. Rept. **173** (1989) 173.
 - [8] E. Witten, Nucl. Phys. B **160** (1979) 57.
 - [9] W. Hasenfratz and R. Klein, Physica **89A** (1977) 191.
 - [10] D. K. Campbell, J. F. Schonfeld and C. A. Wingate, Physica **9D** (1983) 1.
 - [11] J. A. Combs and S. Yip, Phys. Rev. B **28** (1983) 6873.
 - [12] J. A. Combs and S. Yip, Phys. Rev. B **29** (1984) 438.
 - [13] S. V. Demidov and D. G. Levkov, JHEP **1106** (2011) 016 [arXiv:1103.2133 [hep-th]].

- [14] A. B. Adib, M. Gleiser and C. A. S. Almeida, Phys. Rev. D **66** (2002) 085011 [arXiv:hep-th/0203072].
- [15] N. Graham, Phys. Rev. D **76** (2007) 085017 [arXiv:0706.4125 [hep-th]].
- [16] R. H. Goodman and R. Haberman, Siam J. Appl. Dyn. Syst. **4** (2006) 1195.
- [17] R. H. Goodman and R. Haberman, Phys. Rev. Lett. **98** (2007) 104103.
- [18] M. Gleiser and R. C. Howell, Phys. Rev. Lett. **94** (2005) 151601 [arXiv:hep-ph/0409179].
- [19] M. Gleiser and R. C. Howell, AIP Conf. Proc. **861** (2006) 501 [arXiv:hep-ph/0604067].
- [20] P. M. Saffin and A. Tranberg, JHEP **0712** (2007) 053 [arXiv:0710.3272 [hep-th]].
- [21] P. M. Saffin and A. Tranberg, JHEP **0708** (2007) 072 [arXiv:0705.3606 [hep-th]].
- [22] Y. Takamizu and K. Maeda, Phys. Rev. D **73** (2006) 103508 [arXiv:hep-th/0603076].
- [23] Y. S. Kivshar, Z. Fei and L. Vazquez, Phys. Rev. Lett. **67** (1991) 1177.
- [24] T. Romanczukiewicz and Y. Shnir, Phys. Rev. Lett. **105** (2010) 081601 [arXiv:1002.4484 [hep-th]].
- [25] P. E. Dorey, Lecture at the *African Institute of Mathematical Sciences* (2009), unpublished.